Aerosol and Air Quality Research, 15: 1514–1524, 1534

ISSN: 1680-8584 print / 2071-1409 online
doi: 10.4209/aaqr.2014.10.0252

Surface and Column-Integrated Aerosol Properties of Heavy Haze Events in January 2013 over the North China Plain

Li Sun[1,3], Xiangao Xia[1,2*], Pucai Wang[1], Renjian Zhang[4], Huizheng Che[5], Zhaoze Deng[1], Ye Fei[1,3], Liang Ran[1], Xiaoyan Meng[6]

[1] *Key Laboratory of Middle Atmosphere and Global Environment Observation (LAGEO), Institute of Atmospheric Physics, Chinese Academy of Sciences, Beijing, 10029, China*
[2] *Collaborative Innovation Center on Forecast and Evaluation of Meteorological Disasters, Nanjing University of Information Science & Technology, Nanjing, 210044, China*
[3] *University of Chinese Academy of Sciences, Beijing, 10049, China*
[4] *Key Laboratory of Regional Climate-Environment for East Asia (RCE-TEA), Institute of Atmospheric Physics, Chinese Academy of Sciences, Beijing, 10029, China*
[5] *Key Laboratory of Atmospheric Chemistry (LAC), Institute of Atmospheric Composition, Chinese Academy of Meteorological Sciences (CAMS), CMA, Beijing, 100081, China*
[6] *China National Environmental Monitoring Center, Beijing, 100012, China*

ABSTRACT

Heavy haze events were recorded over the North China Plain (NCP) during January 2013. The meteorological condition, in-situ measurement, and ground remote sensing of aerosol size distributions and aerosol optical properties were analyzed to study the meteorological effects on surface and column-integrated aerosol loading. Besides special terrain, analysis of meteorological parameters showed that such a long-standing pollution event was attributable to stagnant weather with high humidity, frequent inversion and low wind speed. The monthly average mass concentration of particulate matter smaller than 1.0 μm (PM_1), 2.5 μm ($PM_{2.5}$), and 10 μm (PM_{10}) was 169, 190, and 233 μg/m^3, respectively. High mass fraction of PM_1 (73%) and $PM_{2.5}$ (82%) in PM_{10} indicated the domination of fine mode particles. Increase of the fraction of $PM_{1–2.5}$ during haze events was attributed to the increase of secondary aerosol under high humidity. Two polluted aerosol types (A1, A3) and one background aerosol (A2) were classified based on aerosol optical depth at 440 nm (AOD_{440}) and column-integrated size distributions. The AOD_{440} of cloud/fog processed aerosol (1.43) was about two and seven times larger than that of A1 and A2, respectively. The single scattering albedo at 675 nm (SSA_{675}) of A3 was ~0.93, which was larger than that of A1 (0.85) and A2 (0.80) due to hygroscopic growth under humid environment.

Keywords: Particle size distribution; Size growth; Aerosol optical properties; Heavy haze.

INTRODUCTION

Aerosols can alter the radiation directly by absorbing and scattering incident light. Furthermore, aerosols serve as cloud condensation nuclei to influence the formation, lifetime of clouds and their radiation budgets. It is widely accepted that aerosols are important agents to influence global and regional climate change (IPCC, 2007). In particular, climate changes in China during the past half century such as weaker East Asian monsoon since the 1970s, cooling in the Yangtze Delta region and Sichuan Basin, flooding in South China and drought in North China since the 1970s, and widespread decrease in surface solar radiation and decreasing cloud coverage since the 1960s are suggested to be closely related to an increase in aerosol loading (Li *et al.*, 2007; Li *et al.*, 2011 and references therein), although quantitative assessment of the role of aerosols in regional climate changes requires further study. In addition, aerosols pose a threat to respiratory morbidity and cardiopulmonary health (Cohen and Pope, 1995). The particulate matter (PM) with aerodynamic diameters smaller than 2.5 μm ($PM_{2.5}$) can be suspended in the atmosphere for lengthy periods and can be inhaled into the respiratory system (Cao *et al.*, 2013). Furthermore, particles with aerodynamic diameters smaller than 1 μm play an important role in visibility degradation and radiative interaction (IPCC, 2007).

China has undergone very rapid economic growth since the economic reforms began in the end of 1970s. The

* Corresponding author.
Tel.: 86-10-8299-5071; Fax: 86-10-8299-5073
E-mail address: xxa@mail.iap.ac.cn

country's economic growth has resulted in an increase in energy consumption and thereby air pollution and associated health effects, particularly in megacities (Chan and Yao, 2008). The rapid urban growth and economic development in Beijing during the past three decades, in addition to the significant increase in the number of vehicles in operation, have led to an increasing number of air pollution episodes and low visibility days. A series of laws, regulations, standards, and measures has been implemented to reduce air pollutant emissions and to improve the air quality in Beijing. For example, the municipal government of Beijing launched the "Defending the Blue Sky" project in 1998, when the number of days with clear skies, i.e., days with grade I or II air quality, was only 100. Since 1998, 12 phases of air pollution control measures were adopted and dozens of measures were implemented in planning for the Beijing 2008 Olympic Games (Zhang *et al.*, 2009). For example, high emissions plants were relocated out of Beijing, cleaner production techniques were utilized, and a total industrial emissions control measure was implemented. Significant progress has been made in reducing air pollution as a result of these effective control measures. For example, SO_2 emissions have been successfully controlled, and NO_2 and CO concentrations have not increased even though the number of vehicles has increased by approximately 10% per year in Beijing. It has been estimated that the total emissions of soot particles and non-combustion industrial dust emissions decreased by 60% from 1999 to 2005 (Hao and Wang, 2005). In addition, a slight decreasing trend although not significant was identified for aerosol optical depth (AOD) in Beijing (Xia *et al.*, 2013). However, during January 2013, heavy haze and fog events occurred over east of China, especially the North China Plain (NCP), as a consequence of the combination of anthropogenic emissions, stable weather, and specific terrain. The maximum area enveloped by haze and fog was as high as 1.4 million square kilometers, and about 800 million people were influenced (http://www.nhfpc.gov.cn/). Fig. 1 shows the Moderate Resolution Imaging Spectroradiometer (MODIS) true color images captured from January 6 to January 29. Extensive haze, fog, and low clouds are clearly visible over the southeast region of Yanshan-Taihang Mountain. In order to further understanding of the causes for this heavy air pollution episode and its impact on aerosol optical properties, the meteorological conditions over Beijing and Xianghe were firstly analyzed in detail. Moreover, in situ measurements of aerosol concentration and column-integrated optical properties recorded during January 2013 were studied extensively to reveal the manner in which ground and column-integrated aerosol optical and physical properties varied between haze and no-haze days.

SITE AND MEASUREMENTS

Site

Xianghe is located between two megacities, Beijing and Tianjin, about 50 km southeast of Beijing and 70 km northwest of Tianjin. The two megacities expand fast with economic growth and suffer from heavy anthropogenic emission. Most measurements in this study were conducted in Xianghe (39.754°N, 116.962°E, 8 m above sea level),. Furthermore, the data of aerosol optical properties and radiosonde of meteorological condition measured in Beijing were used. It has been proved that AOD of Xianghe

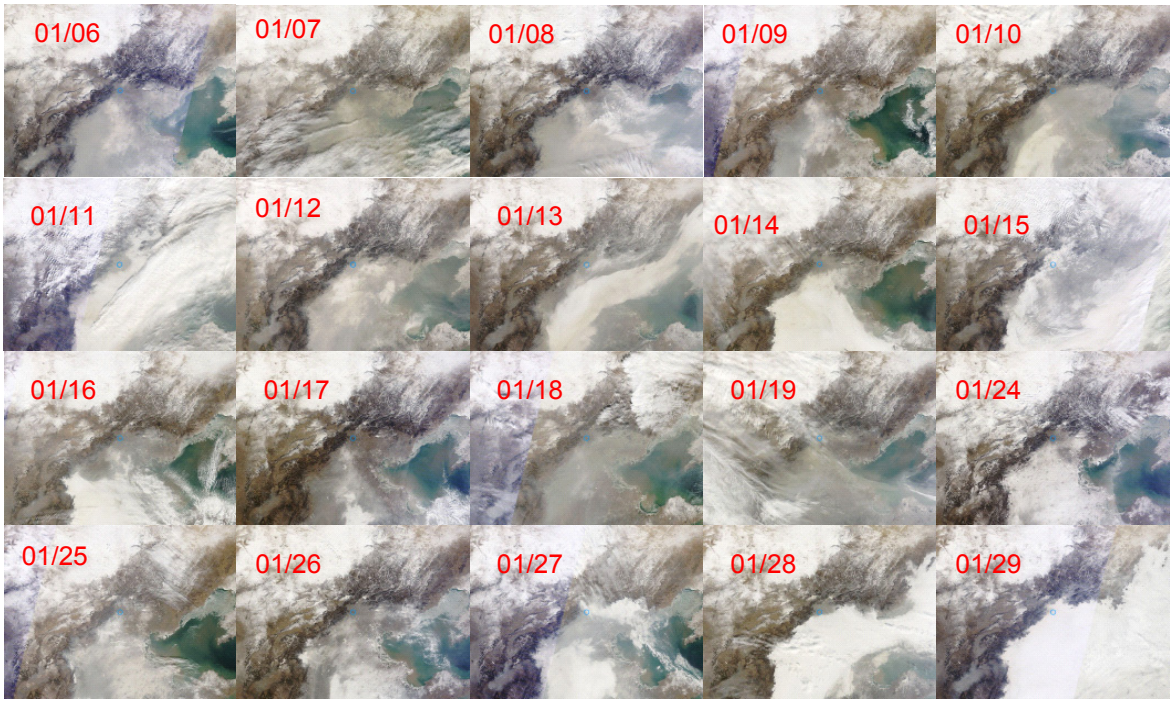

Fig. 1. True-color images centered at the Beijing site (blue circles) captured by Terra and Aqua MODIS during January 2013 (downloaded from http://lance-modis.eosdis.nasa.gov/ imagery/subsets/?project=aeronet).

correlates significantly with that of Beijing, and the difference in AOD between the two sites is negligible (Xia *et al.*, 2005). This result indicates that the aerosol pollution in the NCP is regional in nature.

Measurements

Aerosol Optical Properties

Beijing and Xianghe belong to the Aerosol Robotic Network (AERONET), which is a globally distributed network that provides ground-based remote sensing observation of aerosol optical properties. The CIMEL sun-photometer is the standard instrument used to measure direct and sky radiance at wavelengths ranging from ultraviolet (UV) to near infrared which are used to retrieve the column-integrated parameters such as AOD, refractive index, size distribution, single scattering albedo (SSA), asymmetry factor, and phase function (Holben *et al.*, 2001). Details on aerosol retrievals have been discussed by Dubovik *et al.* (2000). The AERONET data during January 2013 in Xianghe were very limited due to a malfunction of the instrument, therefore, the Level 1.5 AERONET products in Beijing (39.977°N, 116.381°E, 92 m above sea level) that were cloud screened by using Smirnov *et al.* (2000) method were used in the present study. Only 14 days data were available at Beijing AERONET site from January 6 to 28 except for the dates 13, 15, 16, and 19–23 due to cloud contamination.

Aerosol Size Distribution

The size distribution of aerosols at Xianghe during January 2013 was measured by a Scanning Mobility Particle Spectrometer (SMPS, Model 3936, TSI, USA) in combination with an Aerodynamic Particle Sizer (APS, Model 3321, TSI, USA), and mass concentration of aerosols was derived from the size distribution by assuming the density of aerosols ~1.7 g/cm^3 (DeCarlo *et al.*, 2004; Chow and Watson, 2007). A diffusion silicone drier was installed downstream of the aerosol inlet to eliminate the influence of relative humidity (RH) on particle size. SMPS measures the number and size distribution of particles ranging from 10 nm to 700 nm, whereas APS measures those with aerodynamic diameters of 0.5–20 μm. The combination of SMPS and APS provides the number and size distribution of particles in the size range of 10 nm–15 μm in 5 min intervals. PM_1, $PM_{2.5}$, and PM_{10} mass concentration for dry aerosols were calculated on the basis of aerosol size distribution. It should be noted that measurements were not available from January 2 to 4 due to a malfunction of the APS.

Temperature and Humidity Profiles

A 14-channel microwave radiometer (MWR, RPG-HATPRO, Germany) was used to retrieve the temperature and humidity profile in the boundary layer during January 2013 at Xianghe. RPG-HAPRO has 14 receivers that can detect brightness temperatures at 14 wavelengths ranging from 22.2 to 58.0 GHz. The accuracy of the system is within 0.5 K and more details are given in Rose *et al.* (2005). The temperature profile was retrieved from RPG-HATPRO measurements for 25 levels below 2 km with the vertical resolution decreasing from 10 to 200 m from surface to 2 km. The inversion layer was identified when the temperature gradient of the layer was positive. Meanwhile, the altitude of inversion bottom and top was determined to be the minimum and maximum height respectively at which temperature gradient was positive. Temperature gradient of 100 m in inversion (Δ°C/100 *m*) was used to represent the intensity of the inversion layer. Surface temperature, humidity, and wind were measured by AWS on the MWR, which provided important initial values for temperature and water vapor retrieval.

Surface Meteorological Data in January during 2000–2013

To enable a comprehensive understanding of the meteorological conditions in January 2013 over NCP, we compared it with historical meteorological records of Beijing in January from 2001 to 2012. The radiosonde data at Beijing station, recorded twice a day (08:00 and 20:00 LST), were used to calculate the inversion height and occurrence probability (http://weather.uwyo.edu/upperair/sounding.html). Unless specified, all of the parameters analyzed in this paper are the daily averaged values.

RESULTS AND DISCUSSIONS

Temporal Variation of Particulate Matter

Fig. 2 shows the temporal variation of PM mass concentration at various size ranges during January 2013.

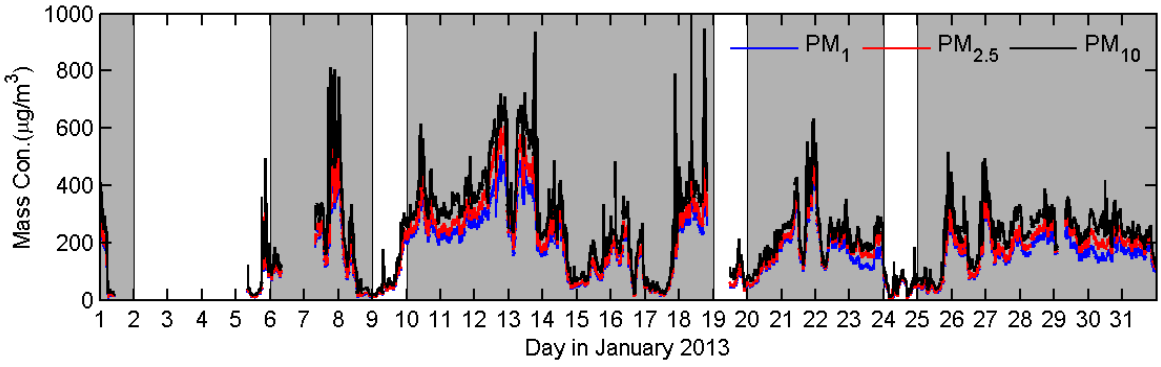

Fig. 2. Temporal variation of particulate matter measured in Xianghe during January 2013. The haze days with daily $PM_{2.5}$ mass concentration larger than 75 μg/m^3 are labeled with gray background.

According to the grade II criterion of National Ambient Air Quality Standard (NAAQS) of China (GB3095-2012)released in 2012, atmosphere is polluted and severely polluted when the daily mean mass concentration of $PM_{2.5}$ are larger than 75 and 250 μg/m^3 respectively. As Fig. 2 shows, there were four long-duration haze episodes that were characterized by daily mean $PM_{2.5}$ > 75 μg/m^3 and maintaining at least two days during the measurement period, including January 6–8, 10–18, 20–23, and 25–31. About 60.7% of measured days in January were lightly polluted and 25% were severely polluted.

The maximum daily average of $PM_{2.5}$ concentration reached 426.6 μg/m^3 on January 12. It was a little larger than those values previously recorded over NCP, such as 200 μg/m^3 by Duan *et al.* (2006) and 357 μg/m^3 by He *et al.* (2001). The minimum value of daily $PM_{2.5}$ concentration, 44.5 μg/m^3, occurred on January 24. Monthly averaged mass concentrations of PM_1, $PM_{2.5}$, and PM_{10} were 169, 190 and 233μg/m^3, respectively. High mass ratio of PM_1, $PM_{2.5}$ in PM_{10} ($PM_1/PM_{2.5}$ ~0.73; $PM_{2.5}/PM_{10}$ ~0.82) indicated the domination of fine mode particles over NCP. Analysis of $PM_{2.5}/PM_{10}$ showed a higher value, 0.81, on haze days than that on no-haze days (0.76). In contrast, the $PM_1/PM_{2.5}$ were 0.90 on haze days, lower than 0.93 on no-haze days.

The high concentration of PM in January 2013 was outstanding even compared with the historical data. Fig. 3 presents the Air Pollution Indexes (API) of January from 2001 to 2013 (downloaded from http://datacenter.mep.gov.cn/). Their calculations are based on the levels of five atmospheric pollutants including SO_2, NO_2, PM_{10}, CO, and O_3. The final score of API is the highest value of these five pollutants. As shown in the Fig. 3, higher monthly means of API in January were observed in 2006 (128) and in 2013 (119). The day number of pollution dominated by PM was 90% and 84% in 2006 and 2013, respectively. A lower value in 2013 was attributed to the clear days of January 1–3 before the haze occurred. The extreme events were more frequent in 2013, and the maximum API reached 406 on January 12, 2013 which is the maximum value for the past 13 years.

Meteorological Conditions

Analysis of the weather maps of NCP during January 2013 showed that the weather condition was featured by the strong zonal circulation at 500 hPa, weak pressure gradient and low wind speed near surface. Fig. 4 shows typical weather maps of severely polluted day on January 12 and a relatively long-standing episode during January 17 and 18. On January 12, the isobars were sparse over NCP indicating the stagnant weather system here. High speed of zonal wind was observed (26 m/s) at 500 hPa (Fig. 4(a)) that favors for the formation and maintenance of stable weather (Wang *et al.*, 2014), while the surface wind speed (Fig. 5(b)) was smaller than 0.2 m/s at 20:00 LST. At 08:00 LST on January 17, the meridional wind was prevalent at 500 hPa with northern wind speed around 20 m/s at upper level. Surface wind speed reached 1.8 m/s and relatively clean air mass transported by northerly winds diluted the pollutants in the boundary layer. The instantaneous concentration of $PM_{2.5}$ was only 27.2 μg/m^3. The meridional wind decreased to 10 m/s at 20:00 LST on January 17 and the surface was dominated by uniform pressure field. The surface wind speed decreased to 1.0 m/s. The instantaneous concentration of $PM_{2.5}$ was 225.3 μg/m^3. After that, the weakening meridional wind was replaced by strong zonal wind (22 m/s) at 08:00 LST on January 18 at 500 hPa. The surface was still dominated by uniform pressure field and the surface wind speed was smaller than 0.1 m/s, the instantaneous $PM_{2.5}$ concentration

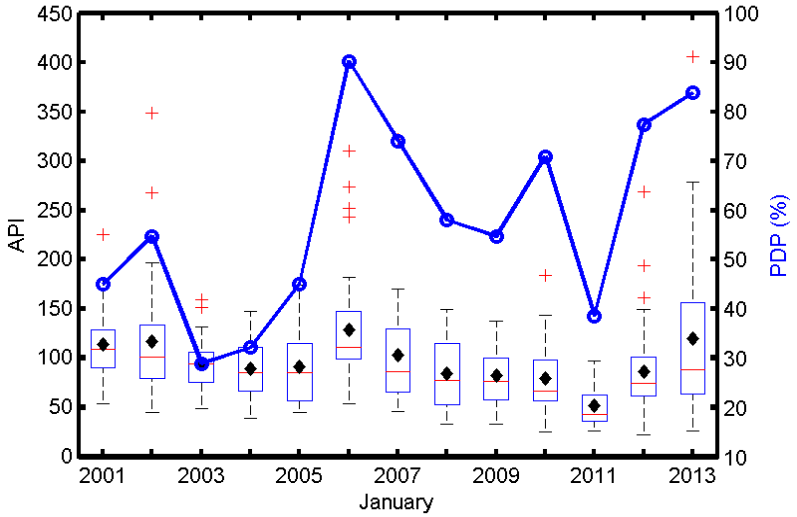

Fig. 3. Box plot of Air Pollution Index (API) and the probability of pollution dominated by particulate matter (PDP) in January from 2001 to 2013 at Beijing. The monthly arithmetic mean value of API is indicated by black diamond and that of PDP is indicated by blue circle. In each box, the red central bar is the median, and the lower and upper limits are the first and third quartiles, respectively. The lines extending vertically from the box represent the spread of the distribution with the length being 1.5 times of the difference between the first and the third quartiles. Observations falling beyond the limits of those lines are indicated by plus symbols.

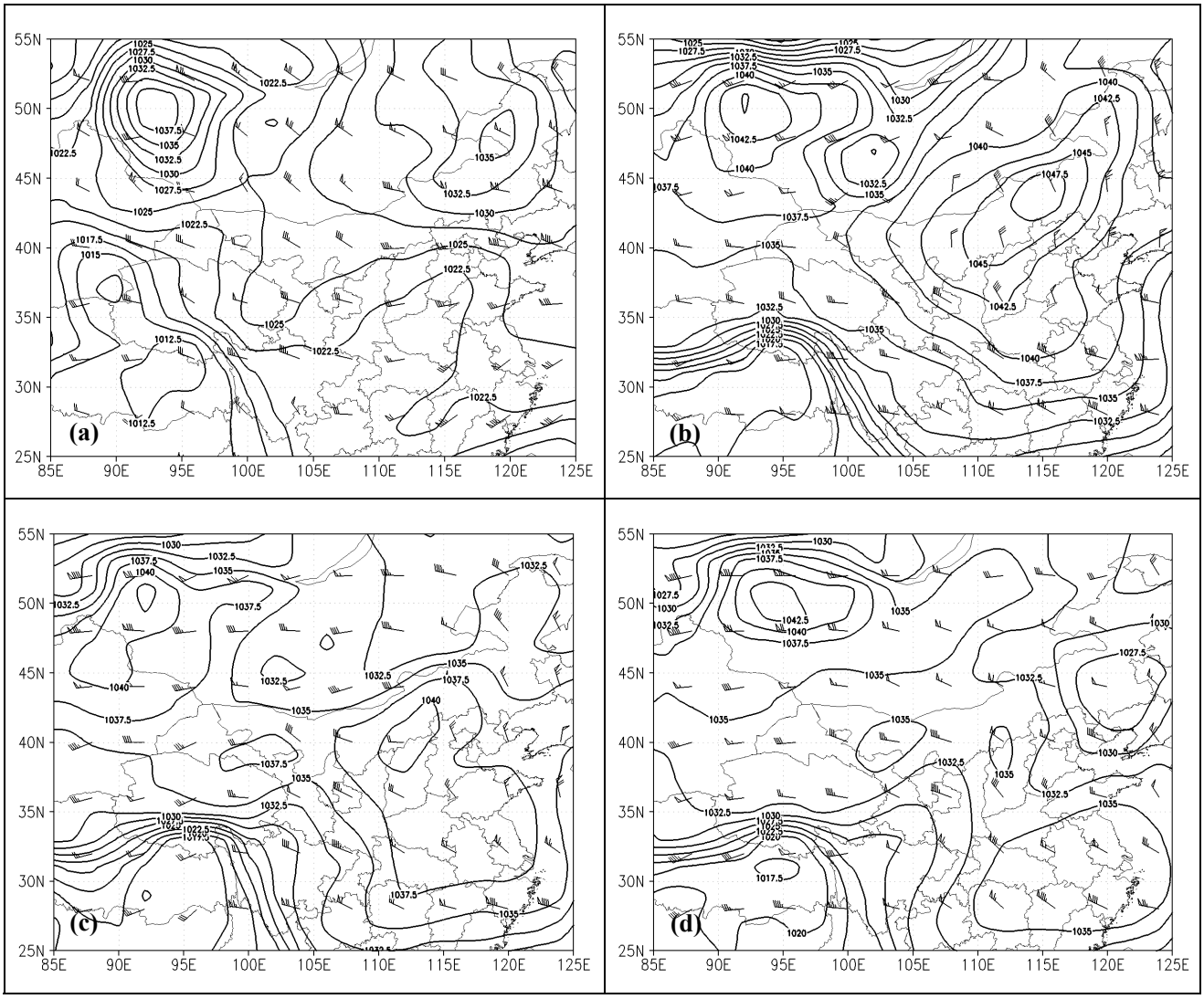

Fig. 4. The sea surface pressure (black line) and wind field at 500 hPa on January 12 at 20:00 LST (a), on January 17 at 8:00 LST (b), 20:00 LST(c), and on January 18 at 8:00 LST (d).

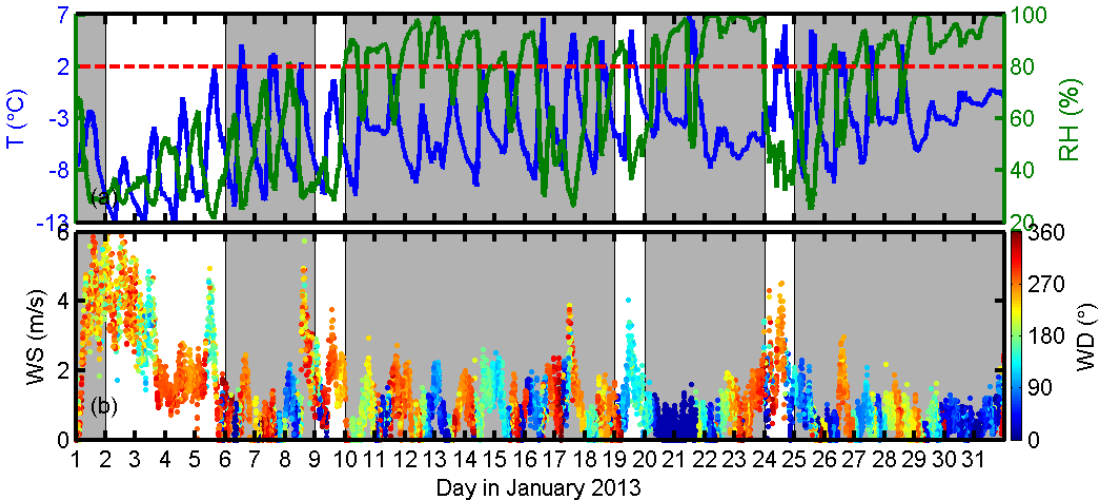

Fig. 5. Temporal variation of surface meteorological parameters including temperature (blue line) and relative humidity (green; the red dotted line indicates RH = 80%) (a), wind speed and wind direction (wind direction is represented by the color of data point and the corresponding color bar is shown right side) (b) in Xianghe during January 2013.

was as high as 692.7 μg/m^3. It can be seen that persistent upper air zonal wind, weak pressure gradient and low surface wind speed contributed to the enhancement of air pollution.

The temporal variation of meteorological variables including temperature, RH, wind speed and direction near surface over Xianghe was shown in Fig. 5. It was shown that polluted days were always characterized by higher RH, lower temperature and wind speed, especially on severely polluted days. It can be speculated that low temperature, wind speed and high RH favored aerosol accumulation over NCP. Fig. 6 shows the surface wind speed and direction dependence of $PM_{2.5}$ mass concentration in Xianghe during January 2013. $PM_{2.5}$ concentrations were mostly higher than 100 μg/m^3 when the wind speed was lower than 2 m/s, indicating strong local emissions. Moreover, the concentration enhanced significantly when the wind came from southern, especially from SSW direction. Therefore, the long-range transport of anthropogenic aerosols by southerly winds also favor for the formation of heavy haze in Xianghe and Beijing.

Temperature inversion is an important factor for air pollution enhancement. It traps pollutants near ground by reducing turbulence and mixing with air aloft (Silva *et al.*, 2007). Fig. 7 shows the temporal variation of inversion heights, temperature and RH profiles over Xianghe within boundary layer during January 2013. As Fig. 7(a) shows, temperature inversions occurred frequently during the measurement period, especially on haze days. For example, on January 12, a severely polluted day, the inversion layer was below 1 km and lasted all day long with mean temperature gradient of 1.0 °C/100 m. High $PM_{2.5}$ mass concentration (326.7 μg/m^3) was observed on January 18 when the inversion with a weaker temperature gradient (0.44 °C/100 m) occurred all day long. On the contrary, on January 24, a clean day, there was no inversion layer at all. Except temperature inversion, abundant water vapor in boundary layer also contributed to the heavy haze. As Fig. 7(b) shows, the values of RH during haze days within boundary layer were mostly greater than 75%.

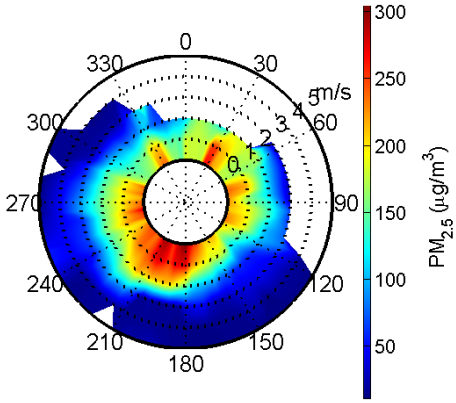

Fig. 6. $PM_{2.5}$ dependence on wind speed and direction in Xianghe during January 2013. $PM_{2.5}$ mass concentration is represented by color for varying wind speeds (radial direction) and wind direction (transverse direction).

Even compared with historical records, the meteorological conditions of January 2013 was unprecedented for such long-duration air pollution. A comparison of surface meteorological observations recorded in January at Beijing during 2001–2013 is presented in Fig. 8. The occurrence probability of atmospheric inversion was calculated from the temperature profiles observed by radiosonde at Beijing station (Fig. 8(b)). As shown in Fig. 8(b), the mean occurrence frequency of the inversion in January during 2001–2012 was ~35%. However, the value reached 70% in January 2013 which was twice the decadal mean. More frequent inversion in January 2013 hindered the upward transportation of aerosols, resulting in a high concentration of particles near the surface. As shown in Fig. 8, the minimum monthly mean temperature (−5.4°C) and wind speed (1.8 m/s) were recorded in January 2013 during the past 13 years, while the maximum RH (61%) was also observed in 2013. All of these factors worked together to favor for the persistent pollution over the NCP.

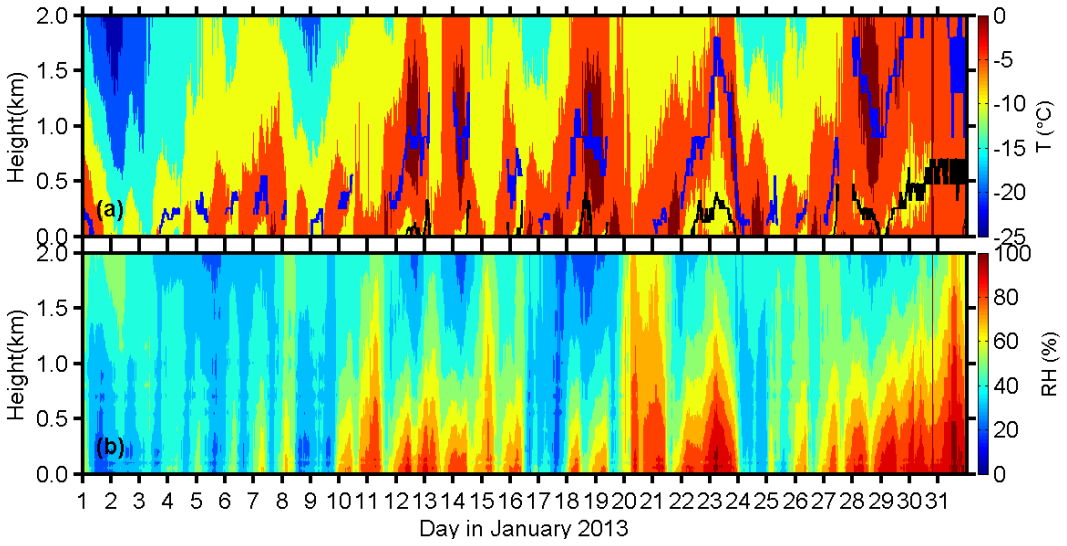

Fig.7. Temporal variation of temperature profile, inversion layer height (bottom: black; top: blue) (a) and relative humidity profile (b) in Xianghe during January 2013.

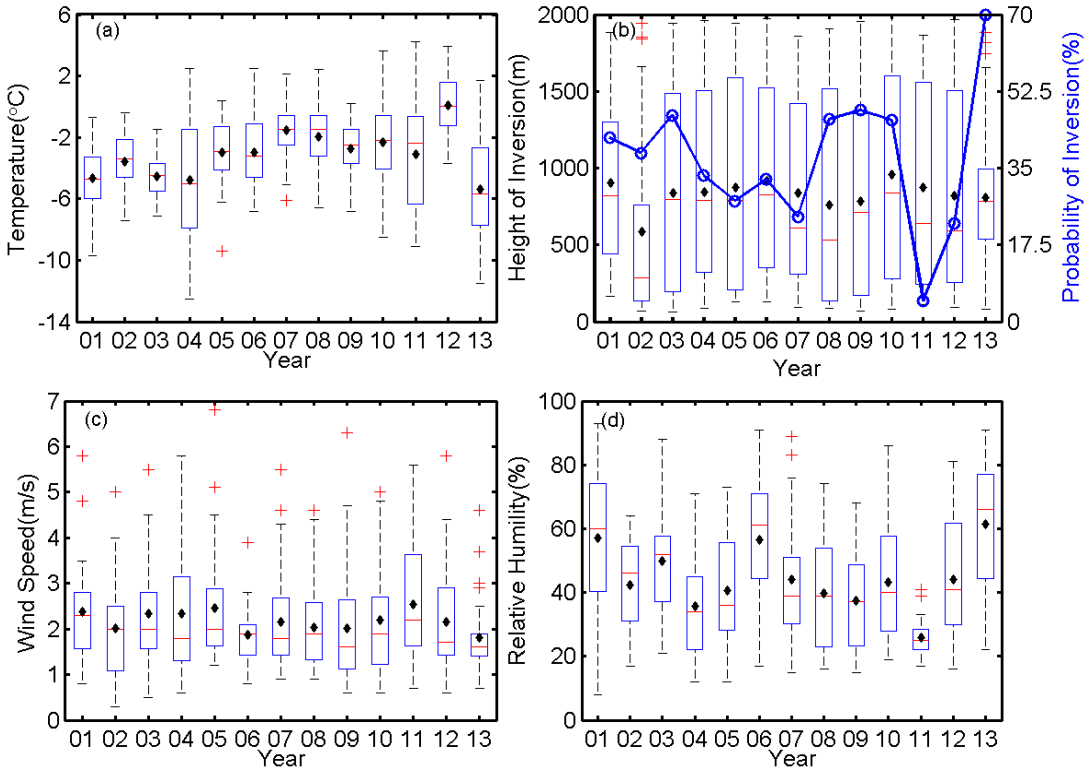

Fig. 8. Box plot of January temperature (a), inversion height and probability of inversion (b), wind speed (c) and relative humidity (d) from 2001 to 2013 over Beijing. The monthly arithmetic mean value is represented by black diamond. In each box, the red central bar is the median, and the lower and upper limits are the first and third quartiles, respectively. The lines extending vertically from the box represent the spread of the distribution with the length being 1.5 times of the difference between the first and the third quartiles. Observations falling beyond the limits of those lines are indicated by plus symbols.

Variation of Aerosol Size Distribution during Haze Events

The Influence of Meteorological Conditions on Aerosol Size

The mass concentration ratio between $PM_1/PM_{2.5}$ and $PM_{2.5}/PM_{10}$ varied with haze and no-hazy days. Daily minimum of $PM_{2.5}/PM_{10}$ (0.68) occurred on January 19 when relatively low RH (62%) and high wind speed (RH ~1.24 m/s) were measured. The maximum $PM_{2.5}/PM_{10}$ value (0.92) occurred on January 22 when high RH (97%) and low wind speed (0.67 m/s) was recorded. The monthly mean ratio of PM_1 to $PM_{2.5}$ was 0.90 (± 0.06), with daily minimum, 0.75, occurred on January 23 (RH ~97%; wind speed 1.05 m/s) and daily maximum, 0.95, occurred on January 6 (RH ~42%; wind speed ~0.80 m/s). It can be seen that the dry aerosols were dominated by fine mode particles. The correlation coefficients between $PM_1/PM_{2.5}$, $PM_{2.5}/PM_{10}$ and meteorological parameters including wind speed and RH were calculated. The results showed that wind speed had little influence on mass concentration ratio between PM_1 and $PM_{2.5}$ (R ~0.04) but a negative correlation with mass concentration ratio between $PM_{2.5}$ and PM_{10} (R ~–0.41). It was likely that the strong wind suspended more coarse particles in the atmosphere and enhanced the proportion of it in PM_{10} but only diluted the mass concentration of fine particles without significant variation of mass ratio between PM_1 and $PM_{2.5}$. The mass concentration ratio of $PM_1/PM_{2.5}$ and $PM_{2.5}/PM_{10}$ showed opposite correlation with RH (R ~–0.44 for $PM_1/PM_{2.5}$; R ~0.59 for $PM_{2.5}/PM_{10}$). These results likely indicated that the growth of PM_{10} with RH elevation was mainly attributed to the growth of $PM_{2.5}$, and the diameters of secondary aerosols formed under high RH mainly ranged from 1 to 2.5 μm. Besides the variation of emission source, the possible reason for the size growth of dry particles were likely attributable to the increasing dissolution of soluble gas, and adhesion or coagulation between particles.

Fig. 9 shows the particle number size distribution (PNSD) normalized by aerosol number concentration and the volume concentration of normalized PNSD of ground-based dry aerosols at different ambient RH ranges. It can be seen that the proportion of large fine particles increased with ambient RH especially at RH lower than 80%. As pointed by Wang *et al.* (2013), the quick transformation mechanism from primary to secondary aerosols, and heterogeneous reaction on the surface of fine mode particles enhanced the hygroscopic growth of particles and thereby the surface area of particles for aqueous reaction during haze and fog that resulted in larger solid particles after drying. Moreover, it has been observed that the concentration of inorganic salts in the RH range from 70% to 80% increased by more than 3 times higher than those in low RH values (Moon *et al.* 2013). The diminishment of coarse particles at high RH condition may be attributable to the sedimentation of coarse mode particles.

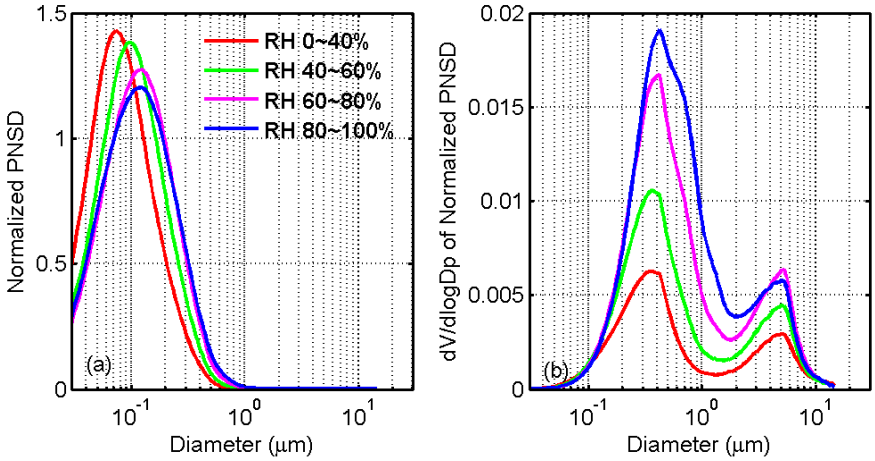

Fig. 9. The particle number size distribution (PNSD) of dry aerosols normalize by aerosol number concentration (a) and volume concentration of normalized PNSD (b) at four ambient relative humidity (RH) ranges of 0–40%, 40–60%, 60–80%, and 80–100% in Xianghe during January 2013.

Size Distribution of Aerosols Modified by Cloud/Fog Process

The aerosols were classified into three types (A1, A2, and A3) according to their size distributions and loadings. A1 and A3 represented polluted aerosols with AOD at 440 nm (AOD_{440}) > 0.4 while A3 was characterized by larger fine particle size as compared to A1. A2 represented background aerosols with AOD_{440} < 0.4. Except on January 24, the Angstrom exponents calculated from AOD 440 and 870 nm ($AE_{440–870}$) were larger than 0.8, indicating the domination of fine mode particles over coarse particles during this episode. The averaged $AE_{440–870}$ was 1.4, 1.1 and 1.0 for A1, A2, and A3 respectively. Fig. 10(c) shows the daily mean size distribution of A3 on January 11, 12, 14 and 28. The outstanding feature is that the peak radii of the fine mode particles were 0.38, 0.38, 0.44 and 0.23μm, respectively, while it was 0.12 ± 0.01 μm for A1 and A2. Large fine mode dominated aerosols (submicron particles) or residual submicron fine mode aerosols retrieved from AERONET have been observed after fog and low-level cloud dissipation at many sites, which indicates the aerosols are modified by fog/cloud process (Dall'Osto *et al.*, 2009; Eck *et al.*, 2012). As shown in Fig. 1, all MODIS satellite images showed low-level cloud or fog either over or near the site for all these days. The smaller daily peak radius of column-integrated aerosol on January 28 was attributable to decay of cloud-processed aerosol, and in turn a larger contribution of smaller-radius aerosol owing to drying of humidified aerosol or fresh aerosol emission (not shown here).

The corresponding daily volume size distribution of dry aerosol measured in Xianghe also showed a larger fine mode peak radius on January 11 and 12 (Fig. 10(f)). The peak radius of dry aerosols was 0.30 and 0.36 μm on January 11 and 12 respectively while it was 0.19 ± 0.01 μm for the other days. Different with January 11 and 12, the peak radius on January 14 and 28 was only 0.20 and 0.21 μm respectively. This was likely attributable to spatial variation of aerosols between Beijing and Xianghe or vertical variation of aerosols.

Considering the size growth of dry particles, it can be seen that physical interaction, aqueous reaction also played an important role in aerosol growth during the haze or fog event besides hygroscopic growth of particles.

Aerosol Optical Properties

Optical properties including AOD, SSA, and aerosol absorption optical depth (AAOD) of A1, A2, and A3 are shown in Fig. 11. Significant differences can be found between these aerosol types. AODs were decreased with wavelength and the averaged AOD_{440} was 0.65 (± 0.13), 0.20 (± 0.03), and 1.43 (± 0.36) for A1, A2, and A3 respectively. Higher scattering efficiency at 675 nm was observed for A1 and A3, and the SSA at 675 nm was 0.85 (± 0.01) and 0.93 (± 0.01) respectively. The high scattering efficiency of A3 could be attributed to the high water content and inorganic salts, especially sulfate, enhancement during haze and fog (Sun *et al.*, 2013). In contrast, high absorbing efficiency (SSA_{675} ~0.80 ± 0.02) with decreasing spectral dependence within the measured wavelength range were observed for A2 indicating the domination of carbonaceous aerosol over Beijing. The AAOD at 440 nm for A1, A2, and A3 was 0.12 (± 0.02), 0.04 (± 0.01), and 0.18 (± 0.04) respectively. Similar with AOD, the relationship between AAOD and wavelength can be described by a power law equation and thereby absorption angstrom exponent (AAE) is derived. The AAE between 440 and 870 nm ($AAE_{440–870}$) of A1, A2, and A3 was 1.7, 0.9 and 1.8 respectively. As pointed by Sokolik and Toon (1999), dust particles aggregated with clay, quartz and hematite exhibit strong absorption in the blue wavelength but lower absorption in visible and infrared spectral range and thereby the value of AAE is generally larger than 2.0 for dust aerosols (Bergstrom *et al.*, 2007; Russell *et al.*, 2010). However, the value of AAE of urban pollution is usually around or slightly larger than 1.0 (Bergstrom *et al.*, 2007). This indicated that both A1 and A3 were mixed aerosol with dust and pollution. Low $AAE_{440–870}$ value and strong

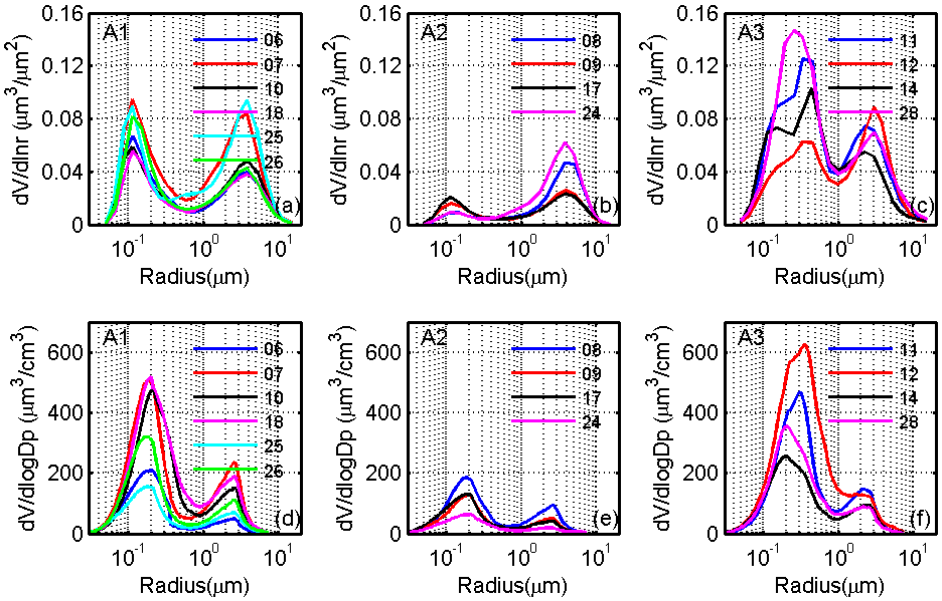

Fig. 10. Daily averaged size distribution of column-integrated aerosols retrieved by AERONET (top panel: a–c) in Beijing and the corresponding size distribution of dry aerosols measured by SMPS and APS (bottom panel: d–f) in Xianghe during January 2013.

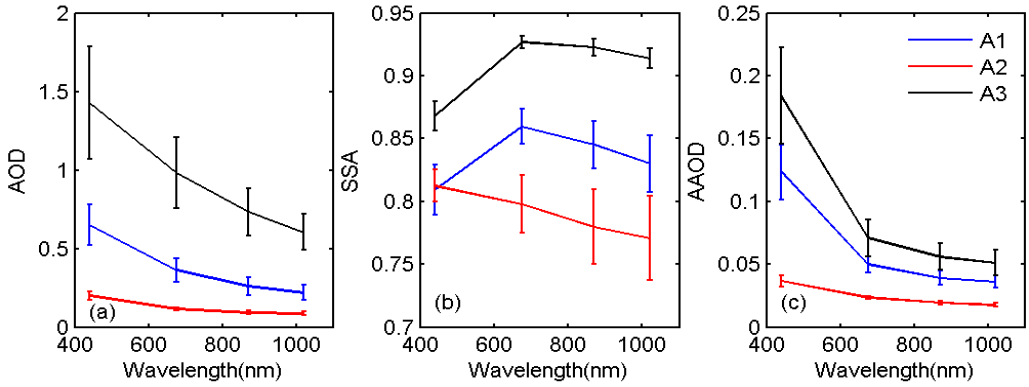

Fig. 11. The averaged aerosol optical depth (AOD) (a), single scattering albedo (SSA) (b), and aerosol absorption optical depth (AAOD) (c) of A1, A2, and A3.

absorption efficiency of A2 indicated that the background aerosols during January 2013 were mainly composited of black carbon.

SUMMARIES AND CONCLUSIONS

Heavy pollution episodes were observed during January 2013 over the NCP. Due to the special terrain, most pollutants were trapped in the southeast region of Yanshan–Taihang Mountain. Prevailing westerly upper zonal wind, weak surface pressure gradient, low surface wind speed, high RH, and frequent inversion provided favorable environment for aerosol accumulation and growth. The monthly averaged RH was as high as 67% (± 24%), and the surface wind speed was only 1.19 ± 1.11 m/s in Xianghe. Compared with the meteorological parameters of Beijing in January from 2001 to 2012, the occurrence frequency of temperature inversion and RH reached the maximum levels in 2013, whereas the surface wind speed and temperature reached the minimum, which contributed to such persistent pollution. Analysis of $PM_{2.5}$ dependence on surface wind speed and direction showed a high $PM_{2.5}$ value under weak wind (< 2 m/s) and southerly wind, indicating the contribution of strong local emission and long-range transport to air pollution over the NCP.

Measurements of aerosols concentration showed high values over the Xianghe site. Expect for those measured on January 5, 9, 19, and 24, the daily mass concentrations of $PM_{2.5}$ were all greater than 75 μg/m^3 and some even greater than 250 μg/m^3, suggesting heavy pollution over the NCP. The maximum daily averaged $PM_{2.5}$ concentration, 426.6 μg/m^3, occurred on January 12 and was higher than that in the historical records. The monthly averaged PM_1, $PM_{2.5}$, and PM_{10} were 169, 190, and 233 μg/m^3 respectively. High mass concentration ratios (PM_1/PM_{10} ~0.73; $PM_{2.5}/PM_{10}$ ~0.82) demonstrated the domination of fine mode particles during the haze period.

The mass ratio of $PM_{2.5}/PM_{10}$ showed a positive correlation with RH while that of $PM_1/PM_{2.5}$ was opposite (R ~0.59 for $PM_{2.5}/PM_{10}$; R ~–0.44 for $PM_1/PM_{2.5}$), indicating the secondary formation of particles in range of 1–2.5 μm under high RH. The peak radius of volume size distribution showed an increase with RH elevation. Accordingly, high $PM_{2.5}$ values recorded in January 2013 are partly attributed to aerosol growth under favorable weather conditions such as high ambient RH.

According to the size distribution and loading of column-integrated aerosols, three aerosol types were identified, i.e., A1, A2, and A3. A3 were observed on January 11, 12, 14, and 28 with the peak radius of fine mode aerosols of approximately 0.38, 0.38, 0.44, and 0.23 μm, respectively, whereas the values were approximately 0.12 ± 0.01 μm on other days. Increase of fine mode peak radius was also observed in Xianghe on January 11 and 12 (0.30 μm on January 11, 0.36 μm on January 12 and 0.19 ± 0.01μm on the other days). Significant difference of aerosol optical properties between A1, A2, and A3 were observed. A3 with larger submicron particles was much effective in light extinction and scattering (AOD_{440} ~1.43; SSA_{675} ~0.93) than A1 (AOD_{440} ~0.65; SSA_{675} ~0.85) and A2 (AOD_{440} ~0.20; SSA_{675} ~0.80).

ACKNOWLEDGEMENTS

The research is supported by the National Basis Research Program of China (2013CBB955801), the National Natural Science Foundation (41175031), and the Strategic Priority Research Program (XDA05100300). The author would like to thank Enago (www.enago.cn) for the English language review.

REFERENCES

Bergstrom, R.W., Pilewskie, P., Russell, P.B., Redemann, J., Bond, T.C., Quinn, P.K. and Sierau, B. (2007). Spectral Absorption Properties of Atmospheric Aerosols. *Atmos. Chem. Phys.* 7: 5937–5943.

Cao, J., Chow, J.C., Lee, F.S.C. and Watson, J.G. (2013). Evolution of $PM_{2.5}$ Measurements and Standards in the U.S. and Future Perspectives for China. *Aerosol Air Qual. Res.* 13: 1197–1211.

Chan, C.K. and Yao, X. (2008). Air Pollution in Mega Cities in China. *Atmos. Environ.* 42: 1–42.

Chow, J.C. and Watson, J.G. (2007). Review of Measurement Methods and Compositions for Ultrafine Particles. *Aerosol Air Qual. Res*. 7: 121–173.

Cohen, A.J. and Pope, C.A.I. (1995). Lung Cancer and Air Pollution. *Environ. Health Perspect.* 103: 219–224.

Dall'Osto, M., Harrison, R.M., Coe, H. and Willams, P. (2009). Real-time Secondary Aerosol Formation during a Fog Event in London. *Atmos. Chem. Phys.* 9: 2459–2469.

DeCarlo, P.F., Slowik, J.G., Worsnop, D.R., Davidovits, P. and Jimenez, J.L. (2004). Particle Morphology and Density Characterization by Combined mobility and Aerodynamic Diameter Measurements. Part 1: Theory. *Aerosol Sci. Technol.* 38: 1185–1205.

Duan, F.K., He, K.B., Ma, Y.L., Yang, F.M., Yu, X.C., Cadle, S.G., Chan, T. and Mulawa, P.A. (2006). Concentration and Chemical Characteristics of $PM_{2.5}$ in Beijing China: 2001-2002. *Sci. Total Environ.* 355: 264–275.

Dubovik, O., Smirnov, A., Holben, B.N., King, M.D., Kaufman, Y.J., Eck, T.F. and Slutsker, I. (2000). Accuracy Assessments of Aerosol Optical Properties Retrieved from Aerosol Robotic Network (AERONET) Sun and Sky Radiance Measurements. *J. Geophys. Res.* 105: 9791–9806, doi: 10.1029/2000jd900040.

Eck, T.F., Holben, B.N., Reid, J.S., Giles, D.M., Rivas, M.A., Singh, R.P., Tripathi, S.N., Bruegge, C.J., Platnick, S., Arnold, G.T., Krotkov, N.A., Carn, S.A., Sinyuk, A., Dubovik, O., Arola, A., Schafer, J.S., Artaxo, P., Smirnov, A., Chen, H. and Goloub, P. (2012). Fog- and Cloud-induced Aerosol Modification Observed by the Aerosol Robotic Network (AERONET). *J. Geophys. Res.* 117: D07206, doi: 10.1029/2011JD016839.

Hao, J. and Wang, L. (2005). Improving Urban Air Quality in China: Beijing Case Study. *J. Air Waste Manage. Assoc.* 55: 1298–1305.

He, K., Yang, F., Ma, Y., Zhang, Q., Yao, X., Chan, C.K., Cadle, S., Chan, T. and Mulawa, P. (2001). The Characteristics of $PM_{2.5}$ in Beijing, China. *Atmos. Environ.* 35: 4959–4970.

Holben, B.N., Tanré, D., Smirnov, A., Eck, T.K., Slutsker, I., Abuhassan, N., Newcomb, W.W., Schafer, J.S., Chatenet, B., Lavenu, F., Kaufman, Y.J., Vande Castle, J., Setzer, A., Markham, B., Clark, D., Frouin, R., Halthore, R., Karneli, A., O'Neill, N.T., Pietras, C., Pinker, R.T., Voss, K. and Zibordi, G. (2001). An Emerging Ground-based Aerosol Climatology: Aerosol Optical Depth from AERONET. *J. Geophys. Res.* 106: 12067–12097, doi: 10.1029/2001jd900014.

IPCC (2007). Climate Change 2007: The Physical Science Basis, Contribution of Working Group 1 to the Fourth Assessment Report of the IPCC. Cambridge University Press.

Li, Z., Chen, H., Cribb, M., Dickerson, R., Holben, B., Li, C., Lu, D., Luo, Y., Maring, H., Shi, G., Tsay, S.-C., Wang, P., Wang, Y., Xia, X., Zheng, Y., Yuan, T. and Zhao, F. (2007). Aerosol Optical Properties and Their Radiative Effects in Northern China. *J. Geophys. Res.* 112: D22S01, doi: 10.1029/2006JD007382.

Li, Z., Li, C., Chen, H., Tsay, S.C., Holben, B., Huang, J., Li, B., Maring, H., Qian, Y., Shi., G., Xia, X., Yin, Y., Zheng, Y. and Zhuang, G. (2011). East Asian Studies of Tropospheric Aerosols and Their Impact on Regional Climate (EAST-AIRC): An overview. *J. Geophys. Res.* 116: D00K34, doi: 10.1029/2010JD015257

Moon, K., Han, J. and Cho, S. (2013). Physical, Chemical and Optical Properties of Fine Aerosol as a Function of Relative Humidity at Gosan, Korea during ABC-EAREX 2005. *Asian J. Atmos. Environ.* 7: 129–138.

Pillai, P.S., Babu, S.S. and Moorthy, K.K. (2002). A study of PM, PM_{10} and $PM_{2.5}$ Concentration at a Tropical Coastal Station. *Atmos. Res.* 61: 149–167.

Rose, T., Crewell, S., Löhnert, U., Simmer, C. (2005). A

Network Suitable Microwave Radiometer for Operational Monitoring of the Cloudy Atmosphere. *Atmos. Res*. 75: 183–200.

Russell, P.B., Bergstrom, R.W., Shinozuka, Y., Clarke, A.D., DeCarlo, P.F., Jimenez, J.L., Livingston, J.M., Redemann, J., Dubovik, O. and Strawa, A. (2010). Absorption Angstrom Exponent in AERONET and Related Data as an Indicator of Aerosol Composition. *Atmos. Chem. Phys*. 10: 1155–1169.

Silva, P.J., Vawdrey, E.L., Corbett, M. and Erupe, M. (2007). Fine Particle Concentrations and Composition during Wintertime Inversions in Logan, Utah, USA. *Atmos. Environ*. 41: 5410–5422.

Smirnov, A., Holben, B.N., Eck, T.F., Dubovik, O. and Slutsker, I. (2000). Cloud-screening and Quality Control Algorithms for the AERONET Database. *Remote Sens. Environ*. 73: 337–349.

Sokolik, I.N. and Toon, O.B. (1999). Incorporation of Minearlogical Composirion into Models of Radiative Properties of Mineral Aerosol for UV to IR Wavelengths. *J. Geophys. Res*. 104: 9423– 9444.

Sun, Y.L., Wang, Z.F., Fu, P.Q., Yang, T., Jiang, Q., Dong, H.B., Li, J. and Jia, J.J. (2013). Aerosol Composition, Sources and Processes during Wintertime in Beijing, China. *Atmos. Chem. Phys*. 13: 4577–4592, doi: 10.5194/acp-13-4577-2013.

Wang, H., Xu, J., Zhang, M., Yang, Y., Shen, X., Wang, Y., Chen, D., Guo, J. (2014). A Study of the Meteorological Causes of Prolonged and Severe Haze Episode in January 2013 over Central-eastern China. *Atmos. Environ*. 98: 146–157.

Wang, Y., Yao, L., Wang, L., Liu, Z., Ji, D., Tang, G., Zhang, J., Sun, Y., Hu, B. and Xin, J. (2013). Mechanism for the Formation of the January 2013 Heavy Haze Pollution Episode over Central and Eastern China. *Sci. China Earth Sci*. 56: 1–12.

Xia, X., Chen, H., Wang, P., Zong, X., Qiu, J. and Gouloub, P. (2005). Aerosol Properties and Their Spatial and Temporal Variations over North China in spring 2001. *Tellus Ser. B* 57: 28–39.

Xia, X., Chen, H., Goloub, P., Zong, X., Zhang, W. and Wang, P. (2013). Climatological Aspects of Aerosol Optical Properties in North China Plain Based on Ground and Satellite Remote-sensing Data. *J. Quant. Spectrosc. Radiat. Transfer* 127: 12–23.

Zhang, X.Y., Wang, Y.Q., Lin, W.L., Zhang, Y.M., Zhang, X.C., Gong, S., Zhao, P., Yang, Y.Q., Wang, J.Z., Hou, Q., Zhang, X.L., Che, H.Z., Guo, J.P. and Li, Y. (2009). Changes of Atmospheric Composition and Optical Properties over Beijing-2008 Olympic Monitouring Campaign. *Bull. Am. Meteorol. Soc*. 90: 1633–1651.

Received for review, October 28, 2014
Revised, January 13, 2015
Accepted, March 23, 2015